

# Signatures of a Maxwellian Component in Shock-Accelerated Electrons in GRBs

Dimitrios Giannios<sup>★</sup> and Anatoly Spitkovsky

*Department of Astrophysical Sciences, Peyton Hall, Princeton University, Princeton, NJ 08544, USA*

Received / Accepted

## ABSTRACT

Recent particle-in-cell simulations suggest that a large fraction of the energy dissipated in a relativistic shock is deposited into a Maxwellian distribution of electrons that is connected to the high-energy power-law tail. Here, we explore the observational implications of such a mixed thermal-nonthermal particle distribution for the afterglow and prompt emission of gamma-ray bursts. When the Maxwellian component dominates the energy budget, the afterglow lightcurves show a very steep decline phase followed by a more shallow decay when the characteristic synchrotron frequency crosses the observed band. The steep decay appears in the X-rays at  $\sim 100$  sec after the burst and is accompanied by a characteristic hard-soft-hard spectral evolution that has been observed in a large number of early afterglows. If internal shocks produce a similar mixed electron distribution, a bump is expected at the synchrotron peak of the  $\nu f_\nu$  spectrum.

**Key words:** acceleration of particles – Gamma rays: bursts – radiation mechanisms: general

## 1 INTRODUCTION

After the prompt emission phase is over, the relativistic ejecta responsible for the gamma-ray burst (GRB) drive a relativistic shock into the circumburst medium. The afterglow emission that follows the GRB is believed to come from the shocked external medium. Electrons are thought to be accelerated at the shock front and radiate throughout the electromagnetic spectrum via synchrotron and synchrotron-self-Compton (SSC) mechanisms (see Piran 2005 for a review).

Particle acceleration in relativistic shocks is poorly understood. Most of the theoretical studies of GRB afterglows parameterize the distribution of particles downstream of the shock by assuming that a fraction  $\epsilon_e$  of the energy dissipated at the shock goes to accelerating *all* electrons into a pure power-law distribution over a wide range of energies (Paczynski & Rhoads 1993; Sari et al. 1998). The possibility that only a fraction  $\zeta_e$  of the electrons are accelerated and the rest thermalize with temperature  $\Theta \equiv kT/m_e c^2 \sim \Gamma$ , where  $\Gamma$  is the bulk Lorentz factor of the shocked plasma, has also been considered (Eichler & Waxman 2005).

Recent particle-in-cell (PIC) simulations have begun to shed light on the acceleration processes at work in relativistic shocks. The picture that emerges for the particle distribution downstream from the shock is somewhat different than what has been traditionally assumed. Diffusive shock acceleration does appear to operate in such shocks, accelerating a small fraction of particles (few %) into a power-law distribution that carries some  $\sim 10\%$  of the dissipated energy. The rest of the electrons are, however, found to be

heated to temperature  $\Theta \sim \Gamma m_p/m_e$  carrying most of the dissipated energy (Spitkovsky 2008a,b; Martins et al. 2009).

In this work, we explore the observational implications of such a mixed thermal-nonthermal particle distribution. We show how the synchrotron emission spectrum and lightcurves are modified compared to conventional afterglow models. We suggest that the spectral and temporal properties of the early X-ray lightcurves that show very steep decay may be produced with such a particle distribution. We also briefly discuss the possible implications of a mixed electron distribution on the prompt GRB emission.

## 2 MODELING THE ELECTRON DISTRIBUTION DOWNSTREAM FROM THE SHOCK

The GRB afterglow emission is believed to come from the shock driven by the ejecta into the circumburst medium. Since the afterglow is steadily observed over a wide range of frequencies ranging from the radio to X-rays (Costa et al. 1997; Frail et al. 1997; van Paradijs et al. 1997; and likely extends into the  $\gamma$ -rays), a broad particle distribution downstream of the shock is needed to explain observations (Sari et al. 1998; see also Paczynski & Rhoads 1993; Waxman 1997; Wijers et al. 1997). A power-law distribution in energy for the particle number  $N_e \propto \gamma^{-p}$  with index  $p \sim 2 - 2.5$  is typically inferred (e.g., Waxman 1997; Galama et al. 1998). Particle acceleration through repeated shock crossings is a promising mechanism to accelerate particles to such a distribution (e.g., Galant, Achterberg & Kirk 1999).

Consider a relativistic shock which has a relative Lorentz factor  $\Gamma \gg 1$  between the shocked and unshocked fluid. A rather eco-

<sup>★</sup> E-mail: giannios@astro.princeton.edu (DG)

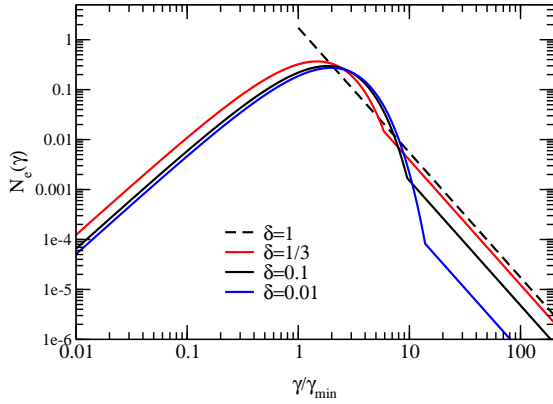


**Figure 1.** The electron-number distribution for different values of the fraction  $\delta$  of the total energy that goes into the power-law component. For  $\delta = 1$ , the pure power-law distribution is reproduced (dashed line). The most recent PIC simulations indicate that  $\delta \sim 0.1$  (solid, black line). For  $\delta \lesssim 1/3$ , the Maxwellian component in the electron distribution is pronounced.

nomical, and popular, parameterization of the particle distribution downstream of the shock assumes that all the electrons are accelerated into a power-law distribution for  $\gamma > \gamma_{min}$ . When  $p > 2$ , most of the energy of the electrons resides at the low end of the distribution. Then,  $\gamma_{min}$  is found from the total available energy per particle assuming that a fraction  $\epsilon_e$  of the energy dissipated by the shock goes into the electrons, resulting in  $\gamma_{min} \sim \epsilon_e \Gamma m_p / m_e$ . In this parameterization, the distribution has a sharp cutoff below  $\gamma_{min}$ .

Eichler & Waxman (2005) considered the possibility of only a fraction of the electrons being accelerated to a nonthermal distribution. The rest were assumed to isotropize and thermalize at a characteristic temperature  $\Theta \sim \Gamma$  given by the upstream kinetic energy of the *electrons* with no extra heating from the ions. In the Eichler & Waxman (2005) approach, the particle distribution is peaked at  $\gamma \sim \Gamma$  and  $\gamma \sim \Gamma m_p / m_e$  with most of the energy carried by the nonthermal component. The nonthermal electrons in this model are responsible for most of the emission (with the possible exception of the early radio afterglow).

Recent PIC simulations of relativistic shocks have revealed both the stochastically accelerated and Maxwellian components in the downstream electron distribution (see Spitkovsky [2008b] and Sironi & Spitkovsky [2009] for simulations of pair shocks, and Spitkovsky [2008a] and Martins et al. [2009] for electron-ion simulations). Simulations of relativistic shocks in weakly magnetized electron-ion plasma show that the thermalized electrons are substantially heated with respect to their upstream bulk flow energy, receiving a large fraction of the dissipated energy from the ions. The electron thermal distribution is smoothly connected to the low end of the power-law component (see Fig. 1). The thermal component is a robust prediction of all simulations, and represents the downstream state of the bulk flow. It can be depleted if the transfer of energy to the power-law component is very efficient. Current simulations show that in shocks that accelerate particles, the power law tail can take of the order of 10–20% of the flow energy. As the present simulations necessarily run for a limited amount of time, it is possible that the steady state has not been achieved yet. Therefore, it makes sense to explore the observational signatures of the mixed thermal-nonthermal distribution for a range of acceleration efficiencies.

In this work, we define the normalized electron distribution downstream of the shock by a continuous function connecting a relativistic Maxwellian to a power-law at  $\gamma = \gamma_{nth}$ :

$$N_e(\gamma, \Theta) = CN_e^{th}(\gamma, \Theta), \quad \text{for } \gamma \leq \gamma_{nth}, \quad (1)$$

$$N_e(\gamma, \Theta) = CN_e^{th}(\gamma_{nth}, \Theta)(\gamma/\gamma_{nth})^{-p}, \quad \text{for } \gamma > \gamma_{nth},$$

where  $N_e^{th}(\gamma, \Theta) = \gamma^2 \exp(-\gamma/\Theta)/2\Theta^3$  is the Maxwell distribution in the  $\Theta \gg 1$  limit (which is of interest here) and  $C$  is a normalization constant. The ratio  $\gamma_{nth}/\Theta$  controls the fraction  $\delta$  of the total energy that resides in the nonthermal component:

$$\delta \equiv \frac{\int_{\gamma_{nth}}^{\infty} \gamma N_e(\gamma, \Theta) d\gamma}{\int_1^{\infty} \gamma N_e(\gamma, \Theta) d\gamma}. \quad (2)$$

Furthermore, we assume that a fraction  $\epsilon_e$  of the energy dissipated in the shock is picked up by the electrons. The average (random) Lorentz factor per particle is

$$\langle \gamma \rangle \equiv \int_1^{\infty} \gamma N_e(\gamma, \Theta) d\gamma = \epsilon_e \Gamma \frac{m_p}{m_e}. \quad (3)$$

Using the last expression with eqs. (1), (2) the electron distribution is determined (i.e.,  $\Theta$  and  $\gamma_{nth}$  can be calculated) after choosing  $\delta$ ,  $\epsilon_e$ ,  $\Gamma$  and  $p$ .

The mixed thermal-nonthermal distribution reduces to the pure power-law for  $\delta = 1$ . In this case  $\gamma_{min} = \gamma_{nth} = (p - 2)\epsilon_e \Gamma m_p / (m_e(p - 1))$  which defines the minimum cutoff of the distribution. In the limit of negligible nonthermal component  $\delta \ll 1$ ,  $\Theta = \langle \gamma \rangle / 3 = \epsilon_e \Gamma m_p / 3m_e$ .

### 3 SYNCHROTRON SPECTRUM

Plasma instabilities that lead to the formation of the collisionless shock are also responsible for the amplification of magnetic fields in the shock transition (Medvedev & Loeb 1999). Whether these small scale fields survive at large distances downstream from the shock is still an open question (Chang et al. 2008, Keshet et al. 2009, Gruzinov 2008; Medvedev & Zakutnyaya 2009). This is, of course, very important, since the fields must remain strong on macroscopic scales for the synchrotron model to explain the afterglow observations (Rossi & Rees 2003, Waxman 2006).

In this paper, we assume that the magnetic fields survive far downstream from the shock and facilitate the synchrotron and SSC radiation. In general, synchrotron dominates the X-ray and softer emission, while inverse Compton (IC) dominates in the  $\gamma$ -ray band (e.g., see Fan et al. 2008 and references therein). Here, we will neglect the IC component and only focus on the new features that appear in the synchrotron emission due to the thermal component in the electron distribution.

We assume that a fraction  $\epsilon_B \sim 10^{-2}$  of the energy dissipated at the shock remains in the magnetic fields at macroscopic distances downstream from the shock. For a fluid moving with  $\Gamma \gg 1$  just behind the shock (in the frame of the central engine), the energy density of the shocked fluid is  $e = 4\Gamma^2 n_{ext} m_p c^2$ , where  $n_{ext}$  is the number density of the external medium (e.g., Sari et al. 1998). The comoving magnetic field strength is thus

$$B^2 = 8\pi\epsilon_B e = 32\pi\epsilon_B \Gamma^2 n_{ext} m_p c^2. \quad (4)$$

Using the standard expressions for synchrotron emission of ultrarelativistic electrons (Rybicki & Lightman 1979), we calculate the spectrum for various values of  $\delta$ . In Fig. 2 we show a “slow

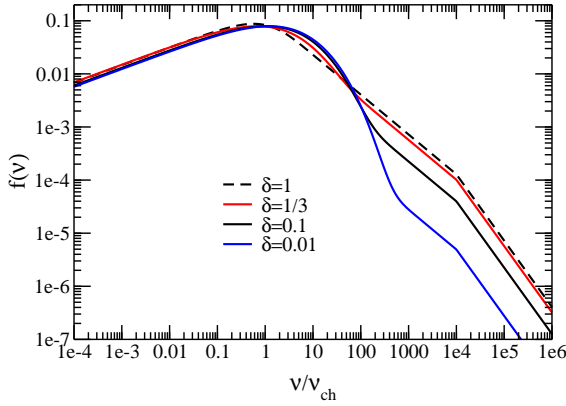


**Figure 2.** Synchrotron spectrum in the case of slow cooling for different values of the fraction  $\delta$  of the energy in the power-law component of the electron distribution. The cooling frequency is taken to be  $\nu_c = 10^4 \nu_{ch}$  ( $\nu_{ch}$  is the characteristic synchrotron frequency). Self-absorption is not included in the calculation.

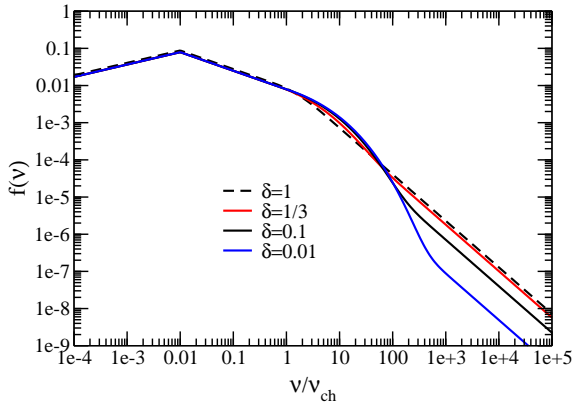


**Figure 3.** Synchrotron Spectrum in the case of fast cooling for different values of the fraction of the energy in the nonthermal component  $\delta$ . The cooling frequency is taken to be  $\nu_c = 0.01 \nu_{ch}$ . The different particle distributions affect the spectral shape at the characteristic synchrotron frequency and the normalization of the high-energy power-law emission.

cooling” case, where the cooling frequency lies above the characteristic synchrotron frequency. A reverse situation, corresponding to the “fast-cooling” case, is shown in Fig. 3. The cooling frequency is defined as the peak synchrotron frequency for electrons whose synchrotron cooling timescale equals the expansion timescale of the system.

The spectra for different  $\delta$  are very similar below the characteristic frequency  $\nu_{ch} = \Gamma \gamma_{min}^2 \nu_{cyc}$ , where  $\nu_{cyc} = eB/2\pi m_e c$  is the cyclotron frequency. The Maxwellian declines fast enough for  $\gamma \ll \Theta$  that the emission at lower frequencies comes from particles close to the peak of the thermal distribution, which is close to the low energy cutoff of the pure nonthermal power law for  $\delta = 1$ . Here we ignore the self absorption which appears in the low-frequency part of the spectrum (typically, radio). We estimate, however, that varying  $\delta$  introduces a weak variation in the self-absorption frequency. Thus, we do not discuss the self-absorption further.

The cooling frequency (or, equivalently, the Lorentz factor of electrons that emit at the cooling frequency) does not depend on the shape of the particle distribution. The difference in spectra due to particle distributions with different  $\delta$  is clearly seen around the characteristic frequency  $\nu_{ch}$ . For  $\delta = 1$  the characteristic frequency appears as a break in the spectrum. For  $\delta \ll 1$ , above the characteristic frequency (determined by the temperature of the thermal component) there is a sharp decline of the emission that is followed by hardening at higher energies. The sharp decline is not described by a power-law spectrum. The hardening corresponds to the emission coming from the nonthermal component of the electron distribution.

This particular shape around the characteristic frequency is reflected in the afterglow lightcurves. When the characteristic frequency crosses the observer band, new afterglow features appear as we discuss in the following section.

#### 4 AFTERGLOW LIGHTCURVES

We consider a blastwave that decelerates due to the accumulation of mass from the circumburst medium. The bulk Lorentz factor of the blastwave depends on the total energy  $E$ , distance  $R$  and the external medium density (and profile)

$$\Gamma(R) \simeq \left( \frac{E}{M_{ext} c^2} \right)^{1/2}, \quad (5)$$

where  $M_{ext} = \int_0^R 4\pi R'^2 n_{ext} m_p dR'$  is the total mass accumulated from the external medium at distance  $R$ .

We focus on two types of external medium: a constant density medium,  $n_{ext} = \text{const}$ , and a wind-like profile  $n_{ext} \propto 1/R^2$ . Note, that we keep  $E$  constant, i.e., we ignore the energy injection that appears to be needed to explain the shallow decay segments of the X-ray lightcurves (Zhang et al. 2006; Nousek et al. 2006). Such inclusion is straightforward but does not affect our main points of discussion.

Although the modeling of the afterglow emission involves several parameters, most of them have been extensively explored in the literature. Here we focus on the new effects on the lightcurves from varying the fraction  $\delta$  of the energy in the nonthermal component. We compute the lightcurves for  $E = 10^{53}$  erg,  $\epsilon_e = 0.3$ ,  $\epsilon_B = 0.01$ , and  $p = 2.5$ , which we will refer to as *reference values* of the parameters. For constant density of the external medium we use  $n_{ext} = 1 \text{ cm}^{-3}$  as a reference value. For the wind case, the density profile is calculated assuming a spherical stellar wind of  $\dot{M} = 10^{-5} M_\odot/\text{year}$  and velocity  $v_w = 10^8 \text{ cm/sec}$  expected from a Wolf-Rayet progenitor (see Li & Chevalier 1999).

In computing the afterglow lightcurves, we use the standard approach described in Sari et al. (1998) and assume a burst at luminosity distance  $d = 10^{28} \text{ cm}$ . In Figs. 4 and 5 we show the resulting lightcurves in the optical and in Fig. 6 the lightcurve at 1 keV.

The lightcurves are very similar for different  $\delta$  until the characteristic frequency crosses the observed band. For  $\delta = 1$  the crossing appears as a single break in the lightcurve. On the other hand, for  $\delta \lesssim 0.1$  there is a steep decline of the lightcurve followed by a break that leads to a more shallow decline. During the steep decline the spectrum shows a characteristic curvature (see next section). The time at which the steep decline is interrupted by a more shallow one occurs when the nonthermal electrons dominate the emission in the observed band. This shape of the lightcurve is a robust expectation from a mixed thermal-nonthermal electron distribution for  $\delta \lesssim 0.1$ .

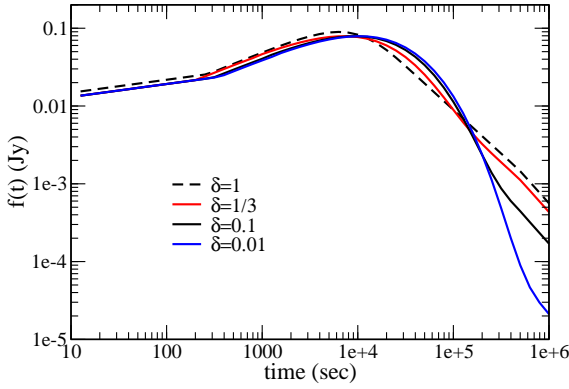


**Figure 4.** Synchrotron lightcurve in the optical band for the reference values of parameters and constant density external medium. The various curves correspond to different values of  $\delta$ . The jet-spreading effects (resulting in a break in the afterglow lightcurve, so called jet break) are not included in the calculation.

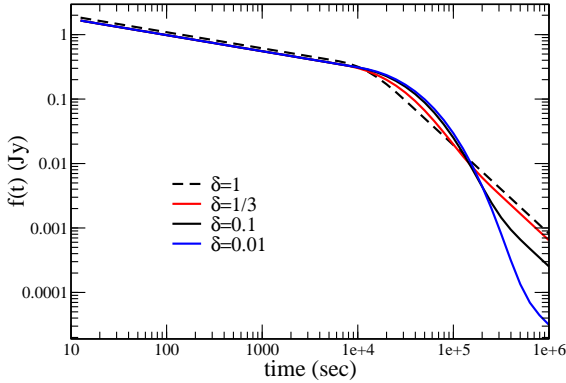


**Figure 5.** Same as Fig. 4 but for the wind-like external medium.

#### 4.1 Application to the early, steep X-ray decay

Very steep decline in the early X-ray afterglow has been frequently observed hundreds of seconds after the GRB (Nousek et al. 2006). The steep decays were initially attributed to off-axis GRB emission (high-latitude model; Kumar & Panaitescu 2000). This interpretation predicts, however, a specific relation between the temporal and spectral power-law indexes during the very steep decay that is not in agreement with that observed in the majority of the afterglows (O’Brien et al. 2006)<sup>1</sup>.

Zhang et al. (2007) did a systematic study of 44 steeply decaying X-ray afterglows for which time resolved spectra are available. They found that 11 X-ray tails did not show significant spectral evolution with time and are compatible with the high-latitude emission

<sup>1</sup> Zhang et al. (2009) modified the high-latitude model by allowing for a non-power-law spectrum upon the cessation of the prompt emission phase. This model can account for the observed spectral evolution during the steep decline of the X-ray afterglows *if* at the end of the prompt emission the spectrum is steepening just above the XRT band.

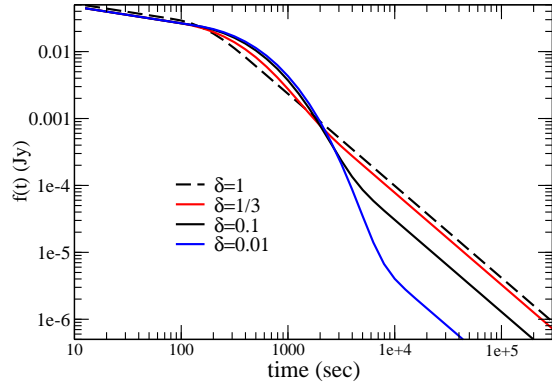


**Figure 6.** X-ray lightcurve for the reference values of parameters and constant density external medium. A wind-like medium results in very similar lightcurves (not shown for clarity of the plot). The jet-spreading effects (resulting in the jet break) are not included in the calculation.

model. The rest show a clear spectral evolution not expected from the high-latitude emission model. Out of those 33 afterglows, 16 have smooth tails (i.e., no flaring activity). The spectral index of the smooth tails showed a characteristic steepening with time in the X-rays from spectral index ( $f_\nu \sim \nu^{-\beta}$ )  $\beta \sim 0.5$  to  $\beta \sim 2$  (see Fig. 2 of Zhang et al. 2007). Moreover, after the very steep decay is over, the spectrum hardens to  $\beta \sim 1.2$ .

All these temporal and spectral features appear naturally when the characteristic frequency from a mixed distribution crosses the X-ray band for  $\delta \sim 0.1$  and depend weakly on the parameters used to model the afterglow emission.

Since  $\nu_{ch} \sim \Gamma \gamma_{min}^2 \nu_{cyc}$ , the characteristic frequency as a function of observer’s time is (ignoring redshift corrections)

$$\nu_{ch} \sim 10^6 \epsilon_{e,0.3}^2 \epsilon_{B,-2}^{1/2} E_{53}^{1/2} t_{obs}^{-3/2} \text{ eV.} \quad (6)$$

For deriving the last expression, we have used Eqs. (4), (5) and that the observer time<sup>2</sup>  $t_{obs} \sim R/4\Gamma^2 c$ . Note that Eq. (6) does not depend on the density of the external medium and approximately applies for both constant density and wind-like media. The characteristic frequency crosses the X-ray band marking the onset of the steep decay time  $t_{sd}$  at

$$t_{sd} \sim 300 \epsilon_{e,0.3}^{4/3} \epsilon_{B,-2}^{1/3} E_{53}^{1/3} \text{ sec} \quad (7)$$

after the burst (with the exact numerical value depending on  $\delta$ ), leading to a steep decline of the lightcurve if  $\delta \lesssim 0.1$  (see Fig. 6).

During the steep decline there is a characteristic softening of the spectrum, which hardens again after the decay enters the power-law phase (see Fig. 7). This spectral evolution with time depends only on the fraction  $\delta$  and not on the external medium. The  $\epsilon_e$ ,  $\epsilon_B$  and  $E$  parameters mainly affect *when* the steep decay (accompanied by the spectral evolution) takes place but not the range over which the spectral index varies.

In Fig. 8 we overplot our model predictions with afterglow observations. We select afterglows with good quality of data from the Zhang et al. (2007) sample that show the typical hard-soft-hard evolution. The observed steepening of the spectrum from  $\beta \sim 0.5$

<sup>2</sup> The expression for  $t_{obs}$  is applicable within a factor of 2 for both wind and ISM external media.

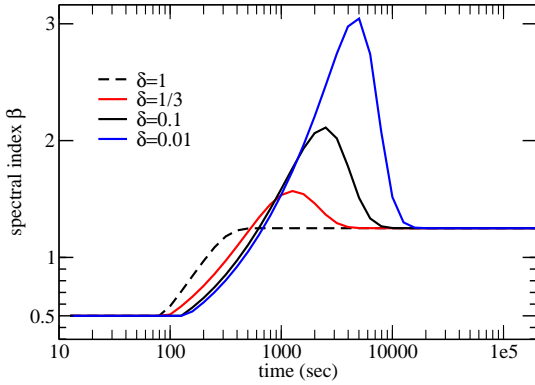


**Figure 7.** Evolution of the spectral index  $\beta$  (where  $f_\nu \sim \nu^{-\beta}$ ) of the  $\sim 1$  keV emission as a function of time for a constant density external medium and for different values of  $\delta$ . A wind profile leads to very similar results. The rest of the parameters are kept to their reference values. The spectral softening takes place simultaneously with the steep decay of the X-ray flux (see Fig. 6).

(characteristic of fast cooling) to  $\beta \sim 2$  appears naturally for  $\delta \sim 0.1$  while the hardening to  $\beta \sim 1$  after the steep decline is over corresponds to the high-energy fast-cooling  $p/2$  segment of the synchrotron spectrum<sup>3</sup>.

Energy injection in the blastwave may be needed to explain the shallow decay of the lightcurve observed after the steep decay phase (Zhang et al. 2006; Nousek et al. 2006). While the energy injection (that is not included in our calculation) affects the temporal evolution of the lightcurves, it does not affect the hard-soft-hard evolution of the spectrum that uniquely reflects properties of the particle distribution. We can, therefore, conclude that in our interpretation of the steep decline,  $\delta$  is constrained to be  $\sim 0.1$  in agreement with recent PIC simulations.

## 5 CONNECTIONS TO THE PROMPT GRB EMISSION

So far we have applied a mixed distribution of accelerated electrons in relativistic shocks to the afterglow emission. The dissipative process responsible for the prompt GRB emission is more uncertain, with internal shocks (Paczynski & Xu 1994; Rees & Meszaros 1994) and magnetic dissipation (Usov 1992; Thompson 1994; Spruit et al. 2001; Lyutikov & Blandford 2003) being the leading candidates. The prompt emission may be the result of synchrotron (Katz 1994), photospheric emission (Eichler & Levinson 2000; Mészáros & Rees 2000; Pe’er, Mészáros & Rees 2006; Giannios 2006) or a combination of the photospheric (that dominates the  $\sim 1$  MeV band) and synchrotron, SSC emission (contributing from the optical to the  $\sim$  GeV band) because of gradual energy release (Giannios 2008).

The internal shock model predicts mildly relativistic collisions. Furthermore, the colliding ejecta may be substantially magnetized. Mildly relativistic collisions of (potentially) magnetized plasma have not been studied in the same detail by PIC simulations.

<sup>3</sup> Note that one of the models shown in Fig. 8 (see yellow line) shows an additional late-time raise of the spectral index from  $\beta = 0.55$  to  $\beta = 1.1$  because of the cooling break crossing the X-ray band.

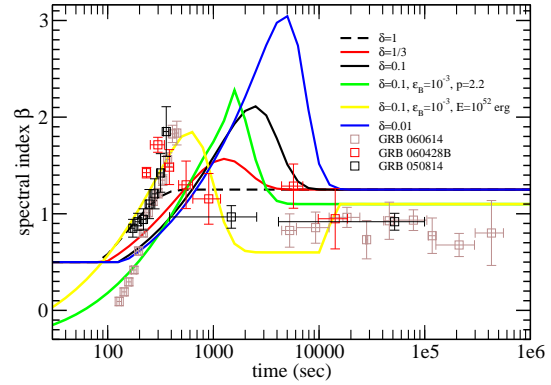


**Figure 8.** The evolution of the spectral index  $\beta$  in the X-rays as a function of time for a constant density external medium as predicted by our model. The dashed, red, black and blue lines are the same as in Fig. 7. The green line shows the model predictions for  $\delta = 0.1$ ,  $\epsilon_B = 10^{-3}$ ,  $p = 2.2$  and the yellow line for  $\delta = 0.1$ ,  $E = 10^{52}$  erg,  $\epsilon_B = 10^{-3}$ , and  $p = 2.2$ . The rest of the parameters are kept to their reference values. Overplotted is the spectral evolution of the GRBs 050814, 060428B and 060614 observed with *XRT* and analyzed in Zhang et al. (2007).

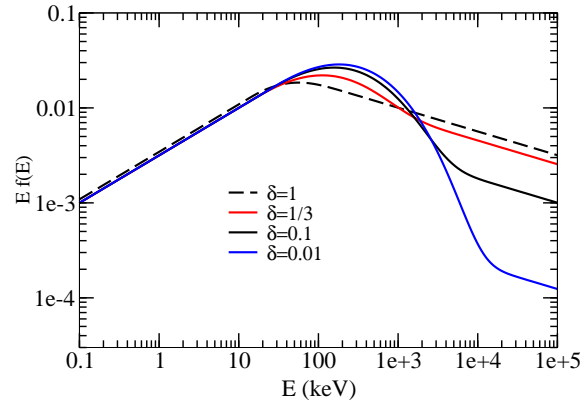


**Figure 9.** The fast-cooling synchrotron spectrum in  $Ef(E)$  representation (arbitrary units) for a shell collision with parameters discussed in the text. A clear thermal-like bump appears when  $\delta \lesssim 0.1$ , followed by the high-energy emission with spectral slope of  $p/2$ . The low-frequency slope is that of fast-cooling electrons, i.e., with spectral slope  $\beta = 1/2$ .

Keeping all these caveats in mind, we explore the possibility that the prompt emission is produced due to synchrotron emission from internal shocks and that the distribution of the downstream particles is a mixed, thermal-nonthermal one. The effect to the prompt emission coming from an injected strong Maxwellian component in the electron distribution has also been discussed in Baring & Braby (2004) (see also Pe’er et al. (2006)).

As an example, we consider two shells ejected with a time difference  $\delta t = 0.1 \delta t_{-1}$  sec. For the ratio of their bulk Lorentz factors  $\Gamma_2/\Gamma_1$  of a few, the shells collide at distance  $R_{IS} \sim \Gamma_{sh}^2 c \delta t / 5$ , where  $\Gamma_{sh}$  is the Lorentz factor of shocked plasma (e.g., Bosnjak et al. 2009). One can check that for  $\epsilon_B = 0.01$ ,  $\epsilon_e = 0.3$ ,  $\Gamma_{sh} = 100$ , the characteristic energy of the synchrotron emission is  $E_{ch} \sim 40$  keV

Fig. 9 shows the fast-cooling synchrotron spectrum for different  $\delta$  for the aforementioned internal shock parameters. For the pure power-law electron distribution ( $\delta = 1$ ), the emission spectrum appears as smoothly connected power laws. A bump at the peak of the  $Ef(E)$  spectrum is pronounced for  $\delta \lesssim 0.1$  in addition to the low- and high-energy power laws. A similar feature has been found by Baring & Braby (2004) for a pronounced Maxwellian component of the downstream electrons (although they adopted a different shape for the particle distribution). Note also that the peak of the spectrum increases by a factor of several for  $\delta \lesssim 0.1$ .

There is evidence for “thermal-like” excess components in a number of bursts (Ryde 2005; Ryde & Pe’er 2009)<sup>4</sup>. Furthermore, a fraction of the bursts show a very steep decline above the peak of the spectrum. These bursts might be connected with very weak nonthermal acceleration in the shocks. The latter is, for example, possible if the colliding ejecta are pre-magnetized with large scale toroidal fields (Sironi & Spitkovsky 2009). On the other hand, a sample of bright bursts does not show any evidence for a significant Maxwellian component in the electron distribution when their spectrum is fitted with a synchrotron model (Baring & Braby 2004). The strength of the bump can be used to constrain  $\delta$  in the synchrotron-internal shock interpretation of the GRB emission.

The spectral slope below the peak of the synchrotron spectrum is that of fast cooling electrons, i.e.  $\beta = 1/2$ . This slope is too soft in comparison to that observed in the majority of the bursts. This is a well-known problem of the synchrotron interpretation of the prompt GRB emission and is not “cured” by the presence of a strong Maxwellian component in the electron distribution. Synchrotron spectra with spectral slope  $\beta \sim 0$  are expected below the synchrotron peak provided that the inverse Compton cooling takes place in the Klein Nishina regime (Derishev, Kocharovskiy & Kocharovskiy 2001; Wang et al. 2009). Harder spectra can be result of photospheric emission and/or heating of the electrons over a timescale much longer than the cooling timescale (slow cooling model; Ghisellini & Celotti 1999; Stern & Poutanen 2004; Pe’er et al. 2006; Giannios & Spruit 2007; Vurm & Poutanen 2009).

## 6 DISCUSSION/CONCLUSIONS

Recent PIC simulations of relativistic shocks show that the electron distribution forms a thermal component downstream of the shock that receives the largest fraction of the dissipated energy in addition to the nonthermal, power-law component (Spitkovsky 2008a,b; Martins et al. 2009). Here, we considered the effect of the thermal component on the afterglow spectra and lightcurves and on the prompt GRB emission.

A strong Maxwellian component introduces new phenomenology when the characteristic frequency of the synchrotron spectrum crosses the observed band. Instead of a break in the lightcurve predicted by the pure power-law model for the electron distribution (e.g., Sari et al. 1998), we find a steep temporal decline followed by a break and a more shallow decay (see Figs. 4, 5, 6). During these phases the spectrum shows a characteristic hard-soft-hard evolution (Fig. 7). The steep decline appears in the X-rays at  $\sim$ hundreds of seconds after the burst *independently* of the external medium density and profile (see Eq. (7)).

<sup>4</sup> Note, however, that the Ryde (2005) analysis fits the spectra with a black-body and a single power-law component while synchrotron emission from the mixed electron distribution results in a bump surrounded by power-law high- and low-energy emission with *different* spectral slopes.

The very steep decay observed in the early X-ray lightcurves has spectral and temporal properties well studied thanks to the XRT on board of *Swift* (Nousek et al. 2006; Zhang et al. 2007). In the majority of bursts, the steep decay shows a characteristic “hard-soft-hard” spectral evolution that is in agreement to that expected from our model when the thermal component in the electron distribution contains  $\sim 10$  times more energy than the nonthermal one (see Fig. 8; in agreement with recent PIC simulations).

Similar steep decline and spectral evolution is expected when the characteristic frequency crosses other bands. From Figs. 4, 5 one can see that the steep decay appears at around 1 day after the burst in the optical band (or slightly later if there is energy injection). During the steep decline, the spectrum is predicted to deviate from a power-law. There are several optical afterglows showing breaks and steep decline at  $\sim 1$  day after the burst. Unfortunately, the time coverage of the optical lightcurves is often sparse and there are other potential physical sources for breaks (end of the energy injection, jet break) that complicate the interpretation of the observations (Liang et al. 2008). It remains to be seen if optical observations support the mixed electron distribution that we propose.

Although the self-Compton emission is not included in our calculations, we expect a similar steep decay signature when the Comptonised component of the characteristic synchrotron frequency  $\nu_{ch}^{IC} \sim \gamma_{min}^2 \nu_{ch}$  crosses the observed band. Depending on parameters, the steep decay can take place at  $\sim 1000$  sec in the  $\sim$ GeV band that is now accessible to observations thanks to the *FERMI* mission (see, e.g., Fan et al. 2008).

Provided that the prompt GRB emission is the result of internal shocks, similar considerations for the distribution of accelerated particles can be applied to the prompt GRB itself. If the large fraction of the energy goes into the Maxwellian component, the synchrotron peak of the prompt emission spectrum should exhibit a “bump” in addition to the typical fast-cooling synchrotron spectrum from nonthermal (power-law) electrons that may be common in GRBs (Ryde 2005), but not universal (Baring & Braby 2004).

## ACKNOWLEDGMENTS

We thank Bin-Bin Zhang for providing the link to observational data. DG acknowledges support from the Lyman Spitzer Jr. Fellowship awarded by the Department of Astrophysical Sciences at Princeton University. AS acknowledges support from the Alfred P. Sloan foundation fellowship and NSF grant AST-080738.

## REFERENCES

- Baring M. G., Braby M. L., 2004, *ApJ*, 613, 460
- Bosnjak Z., Daigne, F., Dubus G., 2009, *A&A*, 498, 677
- Chang P., Spitkovsky A., Arons, J., 2008, *ApJ*, 674, 378
- Costa E. et al., 1997, *Nat*, 387, 783
- Derishev E. V., Kocharovskiy V. V., Kocharovskiy V. V., 2001, *A&A*, 372, 1071
- Fan Y.-Z., Piran T., Narayan R., Wei D.-M., 2008, *MNRAS*, 384, 1483
- Frail D. A., Kulkarni S. R., Nicastro L., Feroci M., Taylor G. B., 1997, *Nat*, 389, 261
- Galama T. J. et al., 1998, *ApJ*, 500, L101
- Gallant Y. A., Achterberg A., Kirk J. G., 1999, *A&AS*, 138, 549
- Ghisellini G., Celotti A., 1999, *ApJ*, 511, L93
- Giannios D., Spruit H. C., 2007, *A&A*, 469, 1



- Giannios D., 2006, A&A, 457, 763  
 Giannios D., 2008, A&A, 480, 305  
 Gruzinov A., 2008, arXiv:0803.1182  
 Eichler D., Levinson A., 2000, ApJ, 529, 146  
 Eichler D., Waxman E., 2005, ApJ, 627, 861  
 Katz J. I., 1994, ApJ, 432, L107  
 Keshet U., Katz B., Spitkovsky A., Waxman E., 2009, ApJ, 693, L127  
 Kumar P., Panaitescu A., 2000, ApJ, 541, L51  
 Li Z.-Y., Chevalier R. A., 1999, ApJ, 526, 716  
 Liang E.-W., Racusin J. L., Zhang B., Zhang B.-B., Burrows D. N., 2008, ApJ, 675, 528  
 Lyutikov M., Blandford R. 2003, arXiv:astro-ph/0312347  
 Martins S. F., Fonseca R. A., Silva L. O., Mori W. B., 2009, ApJ, 695, L189  
 Medvedev M. V., Loeb A., 1999, ApJ, 526, 697  
 Medvedev M. V., Zakutnyaya O. V., 2009, ApJ, 696, 2269  
 Mészáros P., Rees M. J., 2000, ApJ, 530, 292  
 Nousek J. A. et al., 2006, ApJ, 642, 389  
 O'Brien P. T. et al., 2006, ApJ, 647, 1213  
 Paczynski B., Rhoads J. E., 1993, ApJ, 418, L5  
 Paczynski B., Xu G., 1994, ApJ, 427, 708  
 Pe'er A., Mészáros P., Rees M. J. 2006, ApJ, 642, 995  
 Piran, T., 2005, Reviews of Modern Physics, 76, 1143  
 Rees M. J., Mészáros P., 1994, ApJ, 430, L93  
 Rossi E., Rees M. J., 2003, MNRAS, 339, 881  
 Rybicki G. B., Lightman A. P., 1979, Radiative Processes in Astrophysics. Wiley-Interscience Press, New York  
 Ryde F., 2005, ApJ, 625, L95  
 Ryde F., Pe'er A., 2009, ApJ, 702, 1211  
 Sari R., Piran T., Narayan R., 1998, ApJ, 497, L17  
 Sironi L., Spitkovsky A., 2009, ApJ, 698, 1523  
 Spitkovsky A., 2008a, ApJ, 673, L39  
 Spitkovsky A., 2008b, ApJ, 682, L5  
 Spruit H. C., Daigne F., Drenkhahn G., 2001, A&A, 369, 694  
 Stern B. E., Poutanen J., 2004, MNRAS, 352, L35  
 Thompson C., 1994, MNRAS, 270, 480  
 Usov V. V., 1992, Nat, 357, 472  
 van Paradijs J., et al. 1997, Nat, 386, 686  
 Vurm I., Poutanen J., 2009, ApJ, 698, 293  
 Wang X.-Y., Li Z., Dai Z.-G., Mészáros P., 2009, ApJ, 698, L98  
 Waxman E., 1997, ApJ, 485, L5  
 Waxman E., 2006, Plasma Physics and Controlled Fusion, 48, 137  
 Wijers R. A. M. J., Rees M. J., Meszaros, P., 1997, MNRAS, 288, L51  
 Zhang B., Fan Y. Z., Dyks J., Kobayashi S., Mészáros P., Burrows D. N., Nousek J. A., Gehrels, N., 2006, ApJ, 642, 354  
 Zhang B.-B., Liang E.-W., Zhang B., 2007, ApJ, 666, 1002  
 Zhang B.-B., Zhang B., Liang E.-W., Wang X.-Y., 2009, ApJ, 690, L10